Figure 1. Right ventricular dysfunction and myocardial necrosis in response to endurance exercise in *Dsg2*^{mut/mut} mice. (**A**) Percent (%) survival during swim. *P<0.05 vs WT, Mantel-cox survival analysis. *n*-values inset. (**B**) Representative long-axis (top panel) and 2D, B-mode (bottom two panels) echocardiography from exercised WT and *Dsg2*^{mut/mut} mice. Representative of n≥15 mice/genotype. Yellow dashed box, enlarged image of 2D, B-mode middle panel. Note, dilated RV (dashed yellow area, top panel) in *Dsg2*^{mut/mut} mice. (**C**) Percent (%) RV ejection fraction (RVEF) vs %LVEF Pearson's correlation analysis. P-values represent Pearson's correlation between percent RVEF and LVEF within genotype. n≥12 mice/genotype/parameter. (**D, E**) Representative HMGB1 immunostained myocardium from exercised WT and *Dsg2*^{mut/mut} mice, respectively. White arrows; cardiomyocytes (CMs) positive for HMGB1 nuclear localization; yellow arrows; non-CMs positive for HMGB1 nuclear localization. Dotted white lines highlight enlarged areas (i, ii) on right panels. RV, right ventricle. (**F**) Myocardium from exercised *Dsg2*^{mut/mut} mice displayed reduced percent HMGB1+ CMs compared to WT mice. Data presented as mean±SEM, n≥7 mice/ genotype/parameter. *P<0.05 for *Dsg2*^{mut/mut} HMGB1+ CMs vs WT HMGB1+ CMs using One-way ANOVA. Large scale bar = 100μm; small scale bar = 50μm.
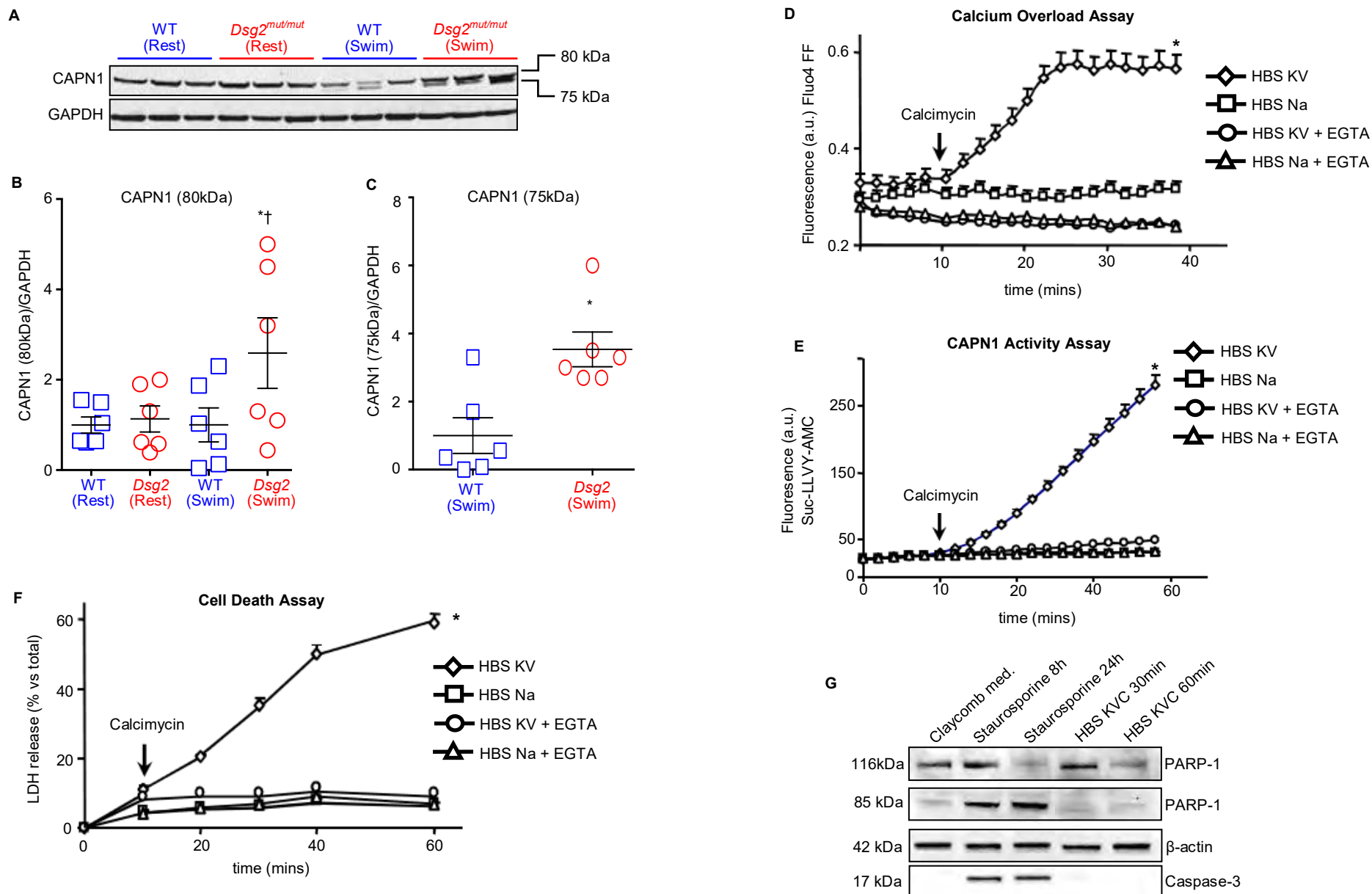
Figure 2. Calpain-1 activation explicates myocyte necrosis. (**A**) Representative Calpain-1 (CAPN1) immunoblot from sedentary (rest) and exercised (swim) mice demonstrated presence of total ([§]80kDa) and active ([||]75kDa) CAPN1, regardless of genotype, in lysates from exercised mice only. (**B**) Exercised $Dsg2^{mut/mut}$ mice displayed increased total myocardial CAPN1 (80kDa) expression compared to all cohorts. *P<0.05 $Dsg2^{mut/mut}$ (swim) vs $Dsg2^{mut/mut}$ (rest); †P<0.05 $Dsg2^{mut/mut}$ (swim) vs WT (swim) using One-way ANOVA. (**C**) Active CAPN1 (75kDa) expression was only observed in myocardial lysates from swimmers, which was potentiated in exercised $Dsg2^{mut/mut}$ mice compared to WT swimmers. *P<0.05 $Dsg2^{mut/mut}$ (swim) vs WT (swim) using 2-tailed, paired t-test. For (**B**) and (**C**) data presented as mean±SEM, n=6 mice/ genotype/cohort. (**D**) HL-1 cells incubated in HBS sodium (HBS Na) or HBS potassium/vanadate (HBS KV) media in the absence or presence of 5mM EGTA; and the Ca^{2+}-ionophore, Calcimycin (1μM, black arrow), to induce calcium (Ca^{2+}) overload. Of note, Ca^{2+}-overload occurred in HL-1 cells containing HBS KV media, only. (**E**) CAPN1 activity, monitored via proteolytic fluorescent-cleavage of a synthetic peptide (Suc-LLVY-AMC), was potentiated in HL-1 cells containing HBS KV media. (**F**) Cell death was detected via lactose dehydrogenase (LDH) release in the media, which was potentiated in HL-1 cells containing HBS KV. (**G**) Representative western blot of Poly [ADP-ribose] polymerase-1 (PARP-1) and the proteolytic fragment of caspase-3 in HL-1 extracts. Cells were treated with Calcimycin (C) in HBS KV medium (HBS KVC) or with staurosporin for the indicated times. PARP-1 and caspase-3 proteolysis, indicating the occurrence of apoptosis, was detected as the appearance of bands at 85 kDa and 17 kDa, respectively. For (**D** -**G**) data presented as mean±St.Dev; n=6 independent experiments/cohort, with n=3 cell culture replicates/condition. *P<0.05 HBS KV vs all cohorts using One-way ANOVA.

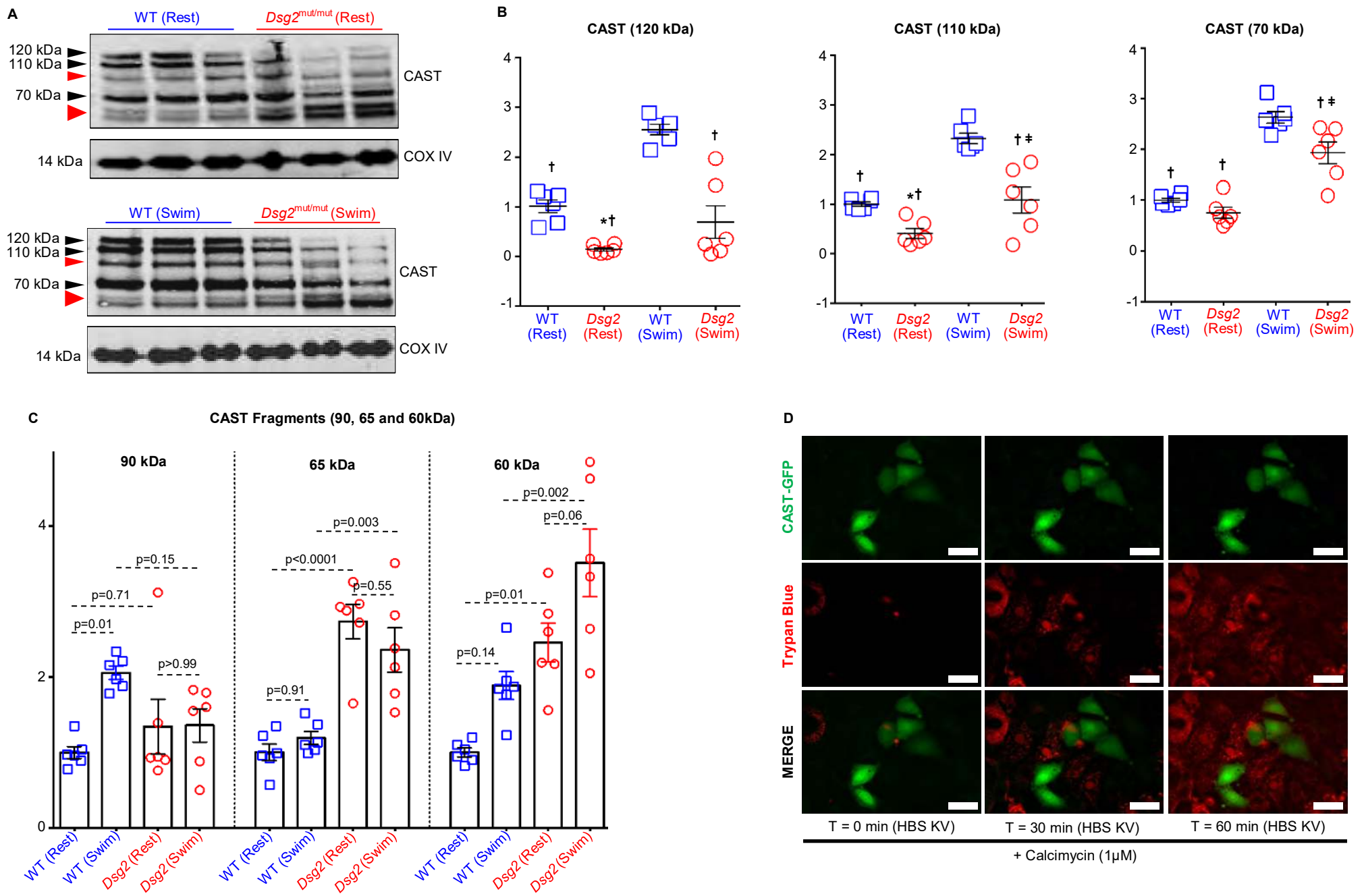**Figure 3. Reduced calpastatin (CAST) levels in *Dsg2*^mut/mut mice and rescue of Ca²⁺ overload-induced cell death via CAST-overexpression.** (**A**) Representative immunoblots probed for changes in calpastatin (CAST) from sedentary (top panel) and exercised (lower panel) mice. Black arrowheads, CAST isoforms; red arrowheads, CAST proteolytic fragments. Immunoblots are representative of n=6 mice/genotype/condition. Mitochondrial cytochrome c oxidase subunit IV (COX IV) was used as a loading control. (**B**) Myocardial lysates from sedentary and exercised *Dsg2*^mut/mut mice showed reduced levels of endogenous CAST isoforms compared to WT counterparts. Data presented as mean±SEM, n=6 mice/genotype/condition. *P<0.05 *Dsg2*^mut/mut (Rest) vs WT (Rest); †P<0.05 for any group vs WT (Swim); and ‡P<0.05 for *Dsg2*^mut/mut (Swim) vs *Dsg2*^mut/mut (Rest) using One-way ANOVA with Tukey's post hoc. (**C**) Expression levels of CAST fragments (90, 65, and 60kDA) from sedentary and exercised cohorts. Data presented as mean±SEM, n=6 mice/genotype/condition, P-values inset using One-way ANOVA with Tukey's post hoc. (**D**) Live-cell imaging of HL-1 cells transfected with a CAST-GFP (green) overexpression construct subjected to HBS KV medium in the absence and presence of Calcimycin (1µM), to induce Ca²⁺ overload. Trypan blue (red) admits red fluorescence via confocal microscopy and is only taken up in dead cells. Of note, HL-1 cells over expressing CAST (green cells) are protected from Ca²⁺ overload-induced cell death (absence of red fluorescence in green cells). Images representative of n=6 independent experiments, with n=3 replicates per cell culture per condition.
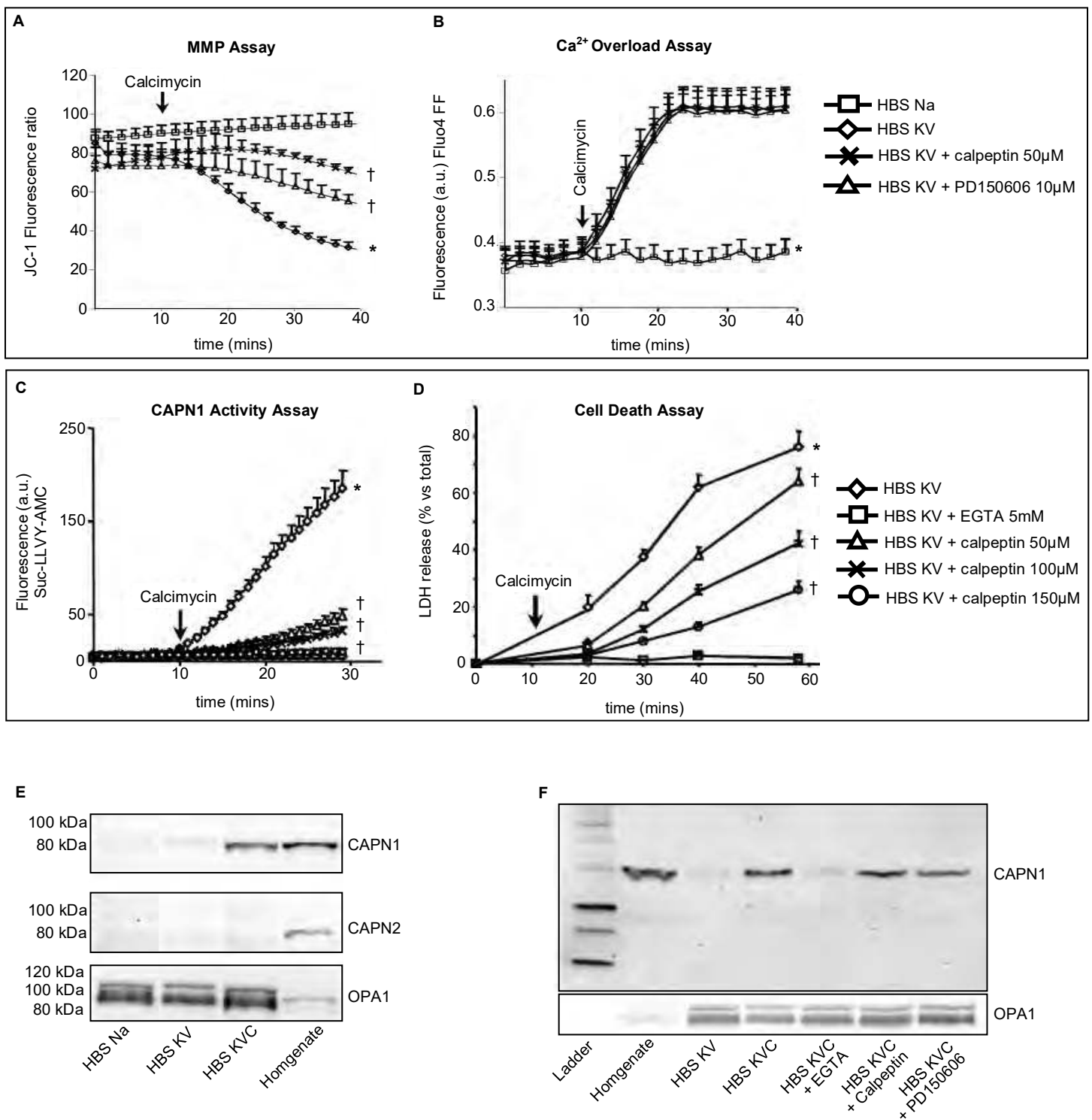
Figure 4. Calpain-1 inhibition markedly reduces mitochondrial dysfunction and cell death following calcium overload. For Figures 4A, B: HL-1 cells were subjected to calcium (Ca^{2+}) overload induced by Calcimycin addition (1 µM, black arrows) in HBS Na medium, and HBS KV medium in the absence or presence of the calpain inhibitors, calpeptin or PD150606. (**A**) Mitochondrial membrane potential (MMP) was monitored using the fluorescent ratiometric probe JC-1 (1.5 µM). *$P<0.05$ for HBS KV vs HBS Na; †$P<0.05$ for HBS KV with either calpeptin and/or PD150606 vs HBS KV using One-way ANOVA. (**B**) Intracellular calcium was monitored by means of Fluo4 FF fluorescence. *$P<0.05$ for HBS Na vs all other conditions; using One-way ANOVA. For Figures 4C, D: HL-1 cells were subjected to Ca^{2+} overload (via Calcimycin, black arrows) in HBS KV medium in the absence or presence of a calpeptin dose-dependent response. (**C**) CAPN1 activity was monitored by proteolysis of the synthetic peptide Suc-LLVY-AMC (25 µM). (**D**) Cell death was detected as LDH release. *$P<0.05$ for HBS KV vs all conditions; †$P<0.05$ for HBS KV with calpeptin (50, 100 and/or 150µM) vs HBS KV, using One-way ANOVA. For (**A-D**) data presented as mean±St.Dev., n=6 independent experiments/cohort, with n=3 cell culture replicates/condition. (**E**) Representative western blots of CAPN1 or CAPN2 in purified mitochondria from HL-1 cells incubated in HBS medium with sodium (HBS Na), HBS medium with potassium and vanadate (HBS KV), and HBS KV subjected to calcium overload (HBS KVC). Cells were incubated under the indicated conditions for 2 min. Equal protein loading was indicated by staining with anti-OPA1 antibodies. (**F**) Representative western blots of CAPN1 in purified mitochondria from HL-1 cells subjected to calcium overload (HBS KVC) in the absence or presence of EGTA (5 mM), calpeptin (50 µM), or PD150606 (10µM). Cells were incubated under the indicated conditions for 2 min. For (**E, F**) immunoblots, representative of n=6 independent experiments/cohort, with n=3 cell culture replicates/condition.
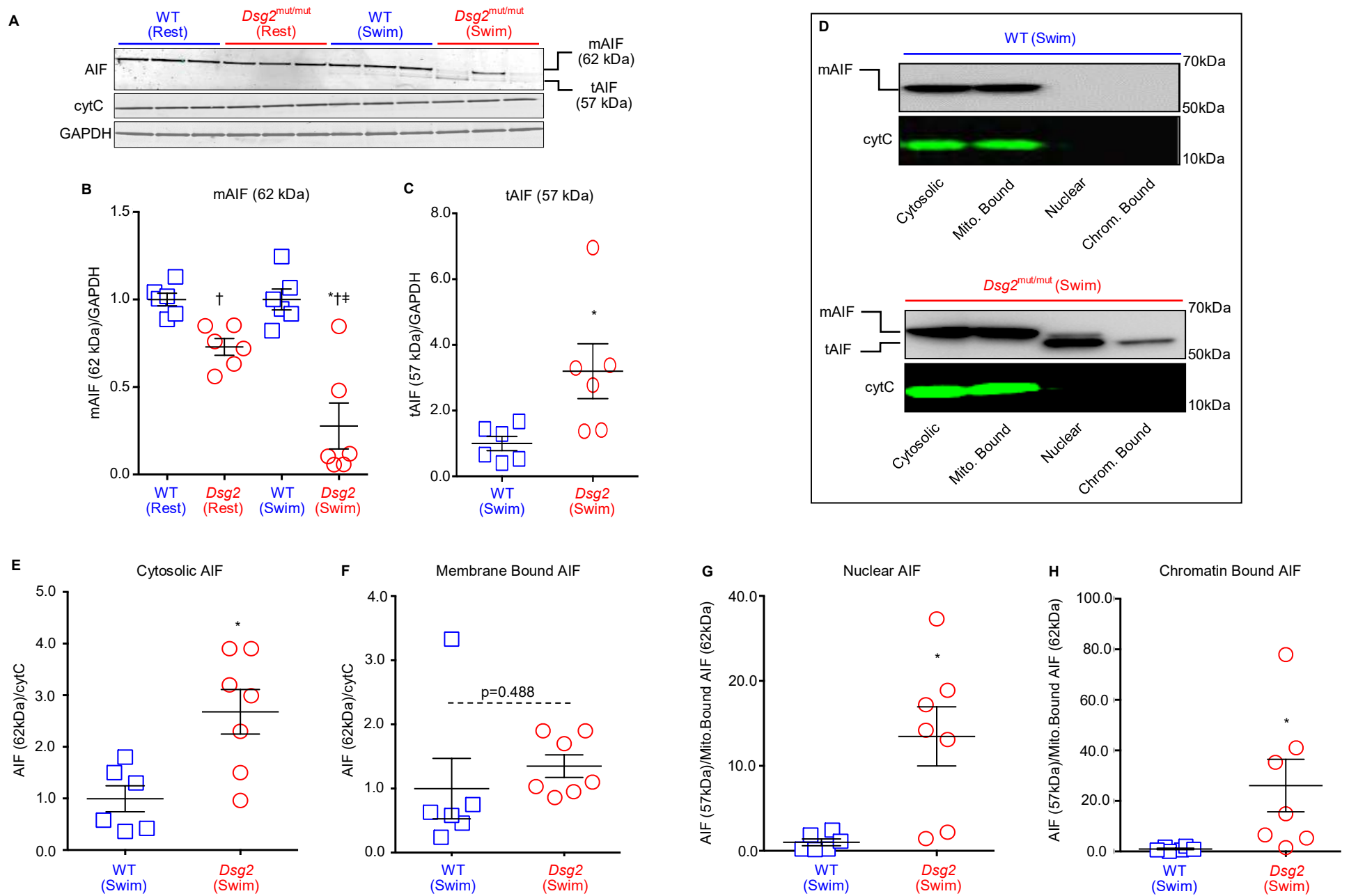
Figure 5. Exercise increases truncation and nuclear localization of myocardial apoptosis-inducing factor (AIF) in *Dsg2*^mut/mut^ mice. (**A**) Ventricular western immunoblots revealed the presence of two distinct bands for apoptosis-inducing factor (AIF), a mature (mAIF, 62kDa) and truncated form (tAIF, 57kDa), in exercised mice, regardless of genotype. (**B**) *Dsg2*^mut/mut^ mice demonstrated reduced myocardial levels of mAIF and (**C**) increased levels of tAIF in response to endurance exercise. Data presented as mean±SEM, n=6/cohort/condition, *P<0.05 vs WT (rest), †P<0.05 vs WT (swim), and ‡P<0.05 vs *Dsg2*^mut/mut^ (rest), using One-way ANOVA for Fig 4B, D. *P<0.05 vs WT (swim) using two-tailed t-test for Fig. 4C. (**D**) Representative western immunoblots from exercised myocardium following subcellular fractionation. Mito. Bound, mitochondrial bound extracts; Chrom. Bound, chromatin-bound extracts. Ventricular lysates demonstrated (**E**) increased levels of cytosolic mAIF, (**F**) no difference in mito-bound mAIF, and increased levels of (**G**) nuclear and (**H**) chromatin-bound tAIF. Data presented as mean±SEM, n≥6/cohort/compartment, *P<0.05 vs WT using 2-tailed t-test.
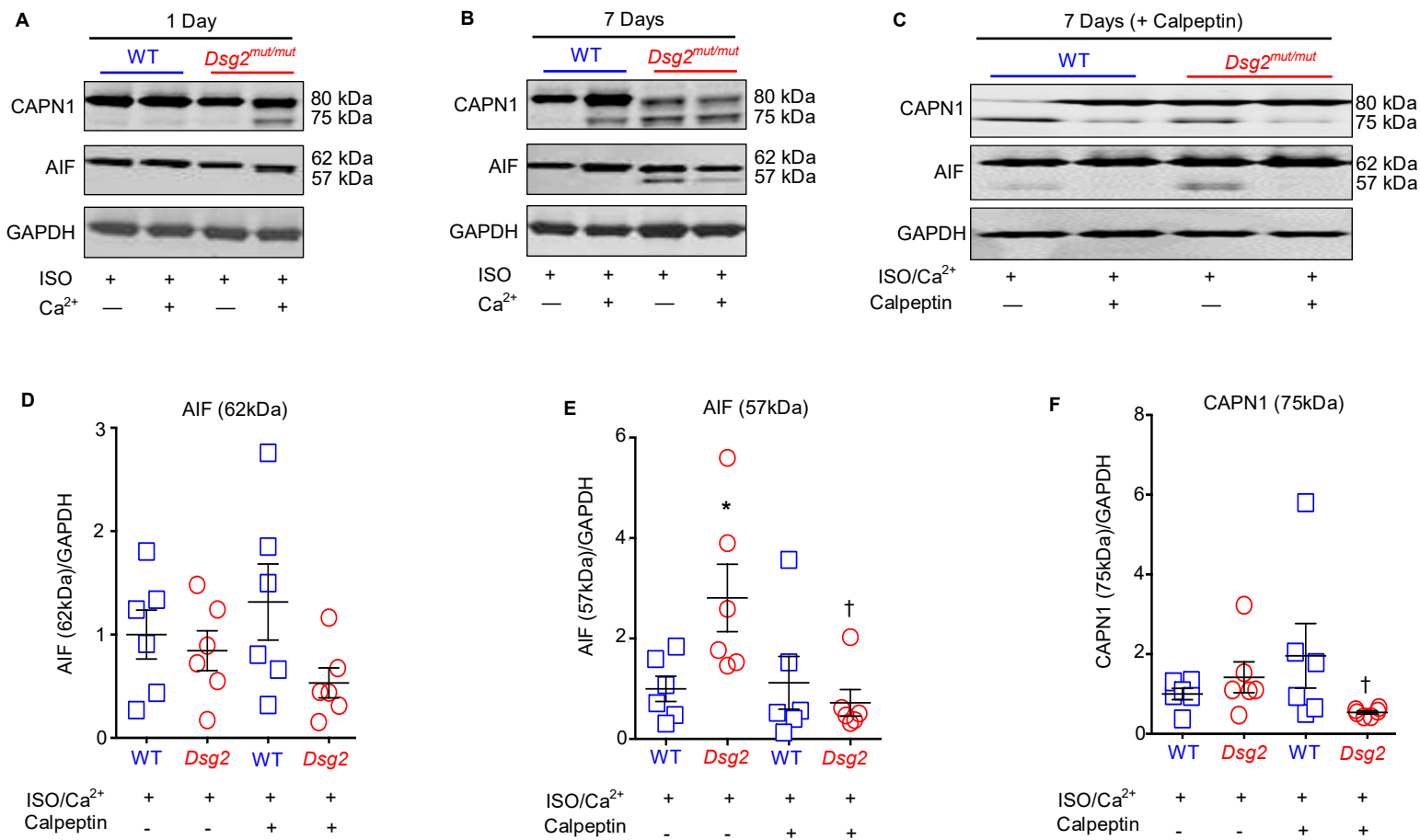
Figure 6. CAPN1-mediated truncation of AIF in ACM cardiomyocytes. Representative immunoblots from WT and *Dsg2*^mut/mut^ ESC-CMs treated for (**A**) 1 or (**B**) 7 days with either 50µM isoproterenol (ISO), 1µM calcium (Ca²⁺), or both ISO and Ca²⁺. Note the formation of truncated AIF (57kDa) in *Dsg2*^mut/mut^ ESC-CMs treated with both ISO-alone and ISO/Ca²⁺ for 7 days. (**C**) Representative immunoblots from WT and *Dsg2*^mut/mut^ ESC-CMs treated for 7 days with 50µM ISO and 1µM Ca²⁺ (ISO/Ca²⁺), in the absence or presence of 50µM calpeptin pretreatment. (**D**) Calpeptin pre-treatment showed a trend towards decreased total AIF (67kDa) in *Dsg2*^mut/mut^ ESC-CMs compared to WT-treated ESC-CMs. (**E**) Calpeptin pre-treatment attenuated both truncated AIF (57kDa) and (**E**) active (75kDa) CAPN1 levels in *Dsg2*^mut/mut^ ESC-CMs. For all figures, data presented as mean±SEM, n=6/genotype/parameter. *P<0.05 ‡P<0.05 untreated *Dsg2*^mut/mut^ ESC-CMs vs untreated WT ESC-CMs; †Calpeptin-treated *Dsg2*^mut/mut^ ESC-CMs vs untreated *Dsg2*^mut/mut^ ESC-CMs using One-way ANOVA.
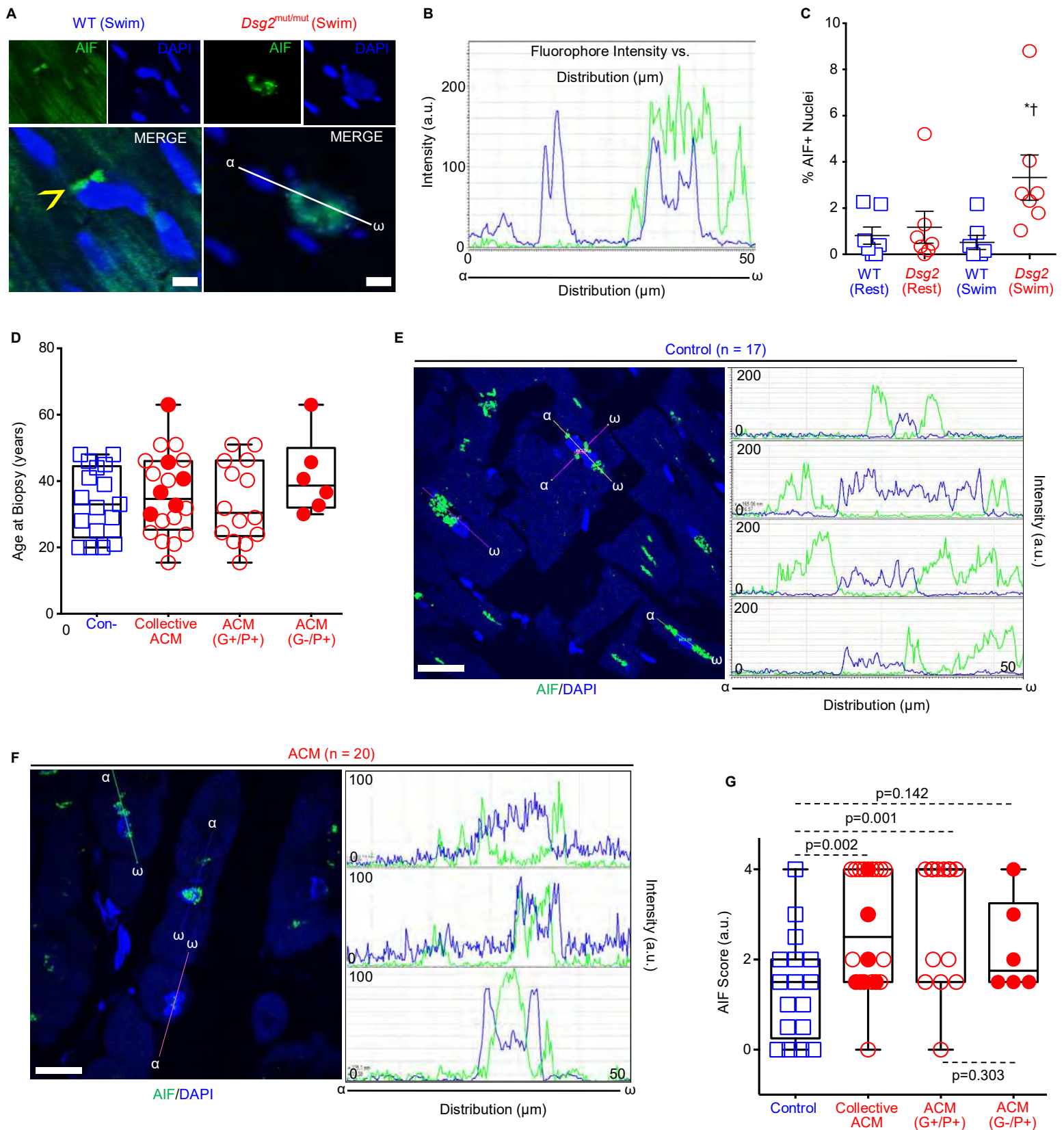
Figure 7. Increased AIF-nuclear localization in ACM myocardium. (**A**) Representative AIF-immunostained myocardium from exercised WT and *Dsg2*^{mut/mut} mice. Yellow arrowhead, perinuclear-AIF. Scale bar = 20μm. (**B**) AIF/DAPI fluorophore intensity vs fluorophore distribution (α-ω), following the methods by Daugas et al. (**C**) Myocardium from exercised *Dsg2*^{mut/mut} mice demonstrated increased percent (%) AIF positive (AIF+) nuclei compared to all cohorts. Data presented as mean±SEM, n=7/genotype/cohort, *P<0.05 *Dsg2*^{mut/mut} (swim) vs WT (Rest), †P<0.05 *Dsg2*^{mut/mut} (swim) vs WT (Swim) using One-way ANOVA. (**D**) Age at biopsy collection. Data presented as mean±SEM, n=17 controls, n=6 ACM (G-/P+), n=14 ACM (G+/P+). (**E, F, left panels**) Representative AIF-immunostained myocardia obtained from ACM patients (n=20) and individuals with no prior history of heart disease (i.e. controls, n=17). (**E, F, right panels**) AIF-nuclear localization was confirmed via *fluorophore distribution vs fluorophore intensity* at 3-10 regions of interest (α-ω). Scale bars = 20 μm. (**G**) AIF pathological scores from ACM patients who met Task Force Criteria (TFC) for ACM (phenotype positive; P+) yet harbored no pathogenic desmosomal variant (genotype negative; G-) and patients who met TFC for ACM (P+) and harbored a pathogenic desmosomal variant (G+), compared against age-matched control myocardium. Of note, only ACM [G+/P+] myocardium showed increased AIF-pathological scores compared to control myocardia. Data presented as mean±SEM, Data presented as mean±SEM, n=17 controls, n=6 ACM (G-/P+), n=14 ACM (G+/P+). P-values inset; using One-way ANOVA.
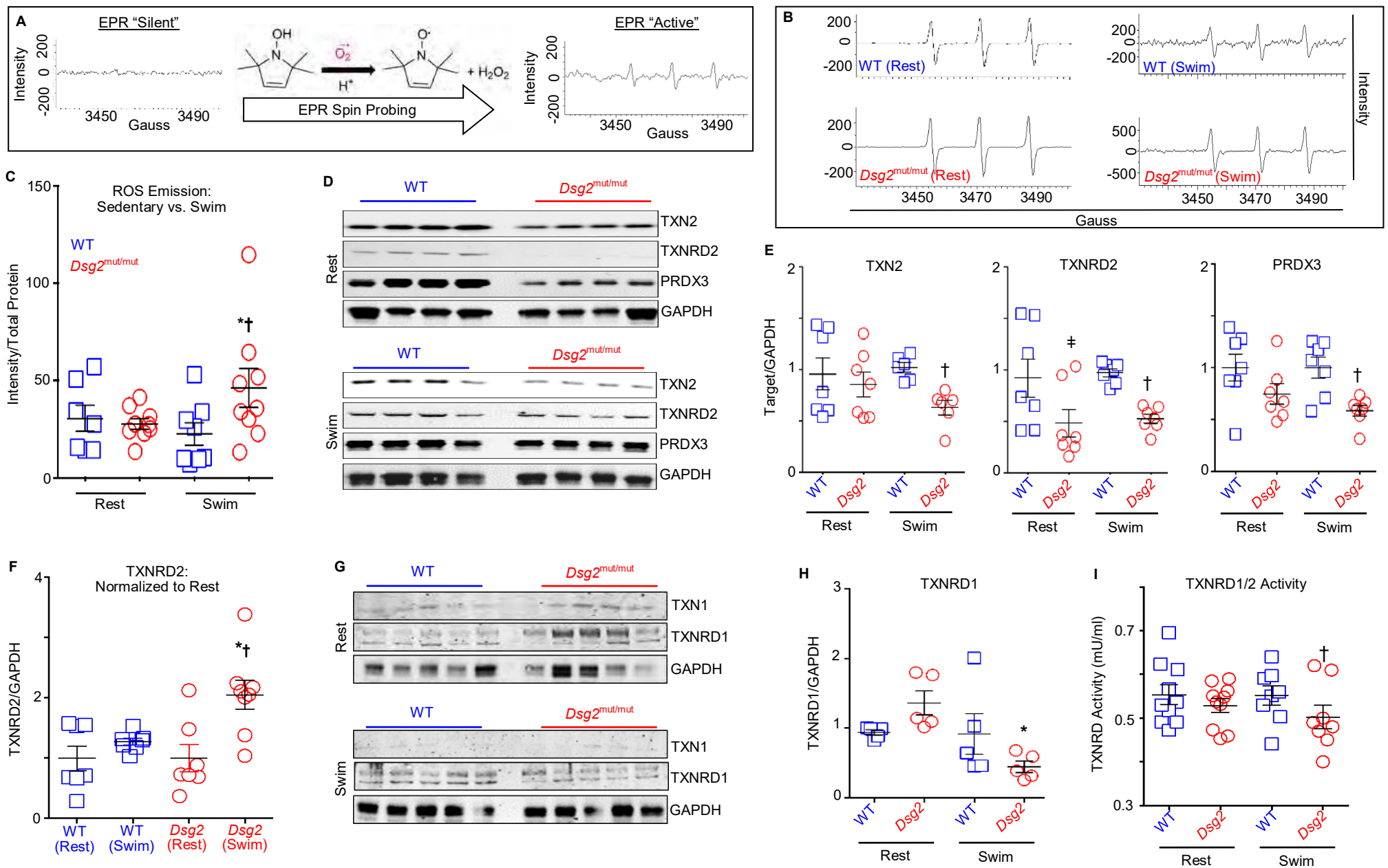
Figure 8. Exercise fails to up-regulate the mitochondrial thioredoxin-2 system in *Dsg2*^{mut/mut} hearts. (**A**) Schematic of ROS emission recordings via electron paramagnetic resonance (EPR) spectroscopy. (**B**) Representative EPR tracings from sedentary (rest) and exercised (swim) cohorts. (**C**) Exercised *Dsg2*^{mut/mut} mice displayed elevated ROS levels in response to exercise. Data presented as mean±SEM, n≥7 genotype/cohort. *P<0.05 *Dsg2*^{mut/mut} (swim) vs *Dsg2*^{mut/mut} (rest); †P<0.05 *Dsg2*^{mut/mut} (swim) vs WT (swim); using One-way ANOVA. (**D**) Western immunoblots from sedentary and exercised cohorts probed for thioredoxin-2 (TXN2), TXN2-reductase (TXNRD2) and peroxiredoxin-3 (PRXD3), normalized to GAPDH. (**E**) Sedentary *Dsg2*^{mut/mut} mice displayed reduced levels of mitochondrial antioxidant protein, TXNRD2, at rest and in response to swimming. Data presented as mean±SEM, n≥6 mice/genotype/parameter. ‡P<0.05 *Dsg2*^{mut/mut} (rest) vs WT (rest); †P<0.05 *Dsg2*^{mut/mut} (swim) vs WT (swim) using One-way ANOVA. (**F**) Exercised TXNRD2 levels normalized to sedentary TXNRD2 levels, within genotype. Note, increased TXNRD2 levels from exercised *Dsg2*^{mut/mut} mice compared to TXNRD2 levels from sedentary *Dsg2*^{mut/mut} mice. Data presented as mean±SEM, n≥7 genotype/cohort, *P<0.05 *Dsg2*^{mut/mut} (swim) vs *Dsg2*^{mut/mut} (rest); †P<0.05 *Dsg2*^{mut/mut} (swim) vs WT (swim); using One-way ANOVA. (**G**) Western immunoblots from sedentary and exercised cohorts probed for thioredoxin-1 (TXN1) and TXN1-reductase (TXNRD1), normalized to GAPDH. (**H**) Sedentary *Dsg2*^{mut/mut} mice showed an increased trend towards elevated TXNRD1 levels, which was markedly downregulated in response to swimming. Data presented as mean±SEM, n=5 genotype/cohort. *P<0.05 *Dsg2*^{mut/mut} (swim) vs *Dsg2*^{mut/mut} (rest) using One-way ANOVA. (**I**) TXNRD1/2 activity was assessed in myocardial homogenates. Of note, myocardial lysates from exercised *Dsg2*^{mut/mut} mice showed reduced TXNRD1/2 activity compared to exercised WT mice. Data presented as mean±SEM, n≥8 genotype/cohort, †P<0.05 *Dsg2*^{mut/mut} (swim) vs WT (swim) using One-way ANOVA.
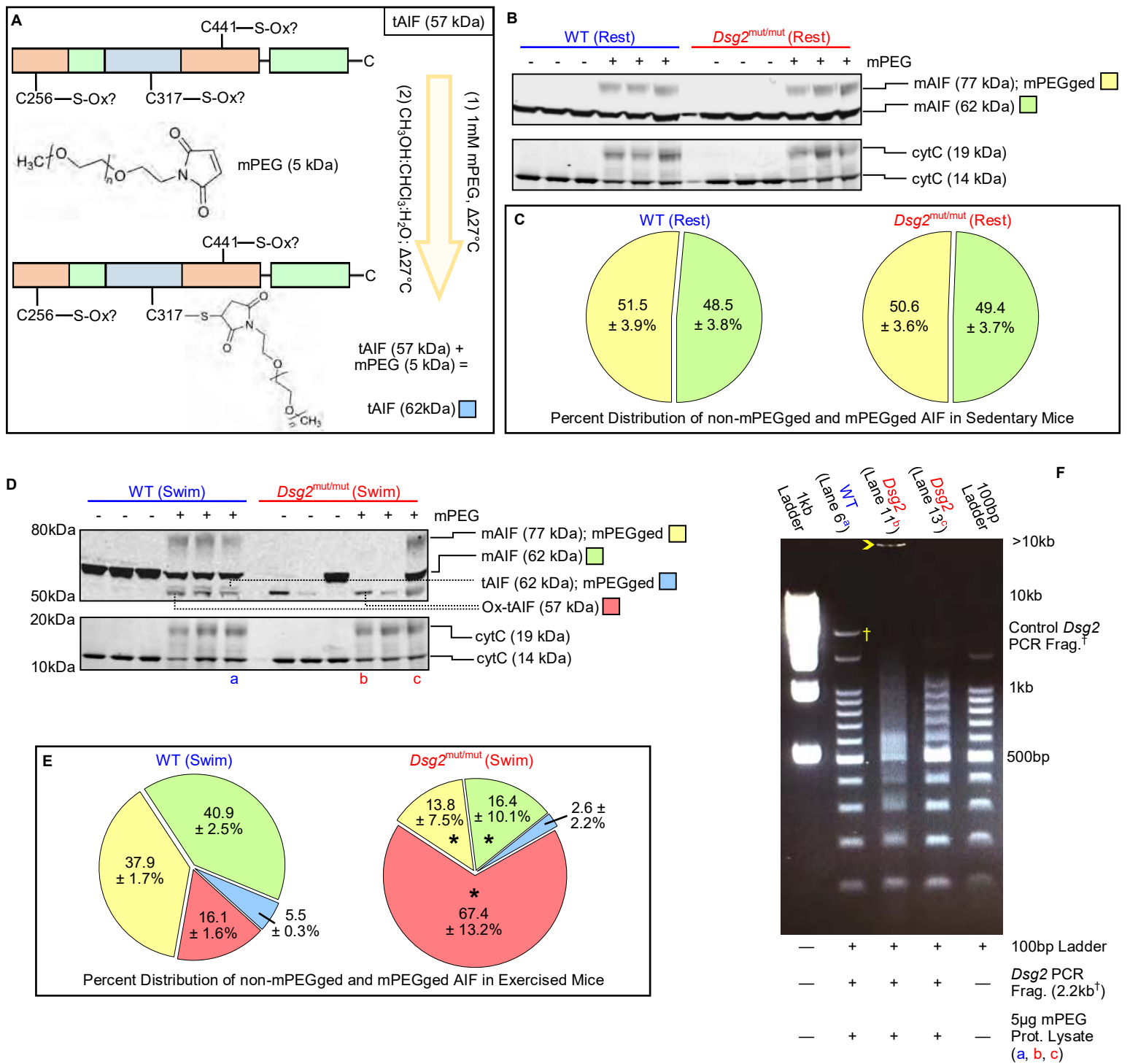
Figure 9. Exercise promotes AIF-oxidation and DNA fragmentation. (**A**) Representative schematic of methoxypolyethylene glycol maleimide (mPEG) treatment. Any non-oxidized cysteine (C256, C317, and/or C441) binds mPEG, adding a 5kDa weight to AIF per cysteine bound-mPEG. (**B**) Representative immunoblots from untreated (-) and 5kDa mPEG-treated (+) lysates from sedentary (rest) cohorts. (**C**) Percent (%) distribution of non-PEGged and mPEGged AIF levels from sedentary mice. No significance to note between non-mPEGged mature AIF (mAIF 62kDa; green) and mPEGged mAIF (mAIF 77kDa, yellow) levels, within and between sedentary cohorts using One-way ANOVA. n=6/genotype/parameter. Data presented in pie-chart form with mean±SEM inset. (**D**) Representative immunoblots and (**E**) percent distribution of non-mPEGged and mPEGged mAIF and truncated AIF (tAIF) levels from exercised (swim) cohorts. n=6 WT mice/parameter, n=7 *Dsg2*[mut/mut] mice/parameter. Data presented in pie-chart form with mean±SEM inset. *P<0.05 for *Dsg2*[mut/mut] vs WT within each respective AIF condition (i.e., *Dsg2*[mut/mut] mAIF 77kDa mPEGged [yellow] levels vs. WT mAIF 77kDa mPEGged [yellow] levels, etc.), using One-way ANOVA with Tukey's post-hoc. Of note, there was a ~4-fold increase in the levels of non-mPEGged (i.e., cysteines have been oxidatively [Ox] modified) Ox-tAIF (57kDa, red) in *Dsg2*[mut/mut] mice compared to Ox-tAIF (57kDa, red) in myocardial lysates from exercised WT mice. For C and E, percent distribution calculated as the expression of each individual mPEGged and/or non-mPEGged AIF levels divided by the sum of all AIF levels times 100. (**F**) Representative DNA retardation assay. Five micrograms [5μg] of mPEG-treated protein lysates (e.g., Fig 9D: lane 6 [a]; lane 11 [b]; and lane 13 [c]) were incubated with a 2.2kb DNA fragment (†Frag.) generated via polymerase chain reaction (PCR) from the WT form of murine *Dsg2* (see Supplemental Figure 6B) and a 100bp DNA ladder. Of note, lysates containing Ox-tAIF (lane 11, [b]) showed DNA retardation ~300bp, no distinct DNA laddering after 500bp, and complete prevention of DNA migration of any DNA fragment over >2kb (yellow arrowhead). In contrast, lysates containing non-oxidized tAIF (lane 13, [c]) showed DNA retardation ~500bp and distinct DNA laddering was still visible from 500-1,000bp. Representative of n≥6mice/genotype/lane.
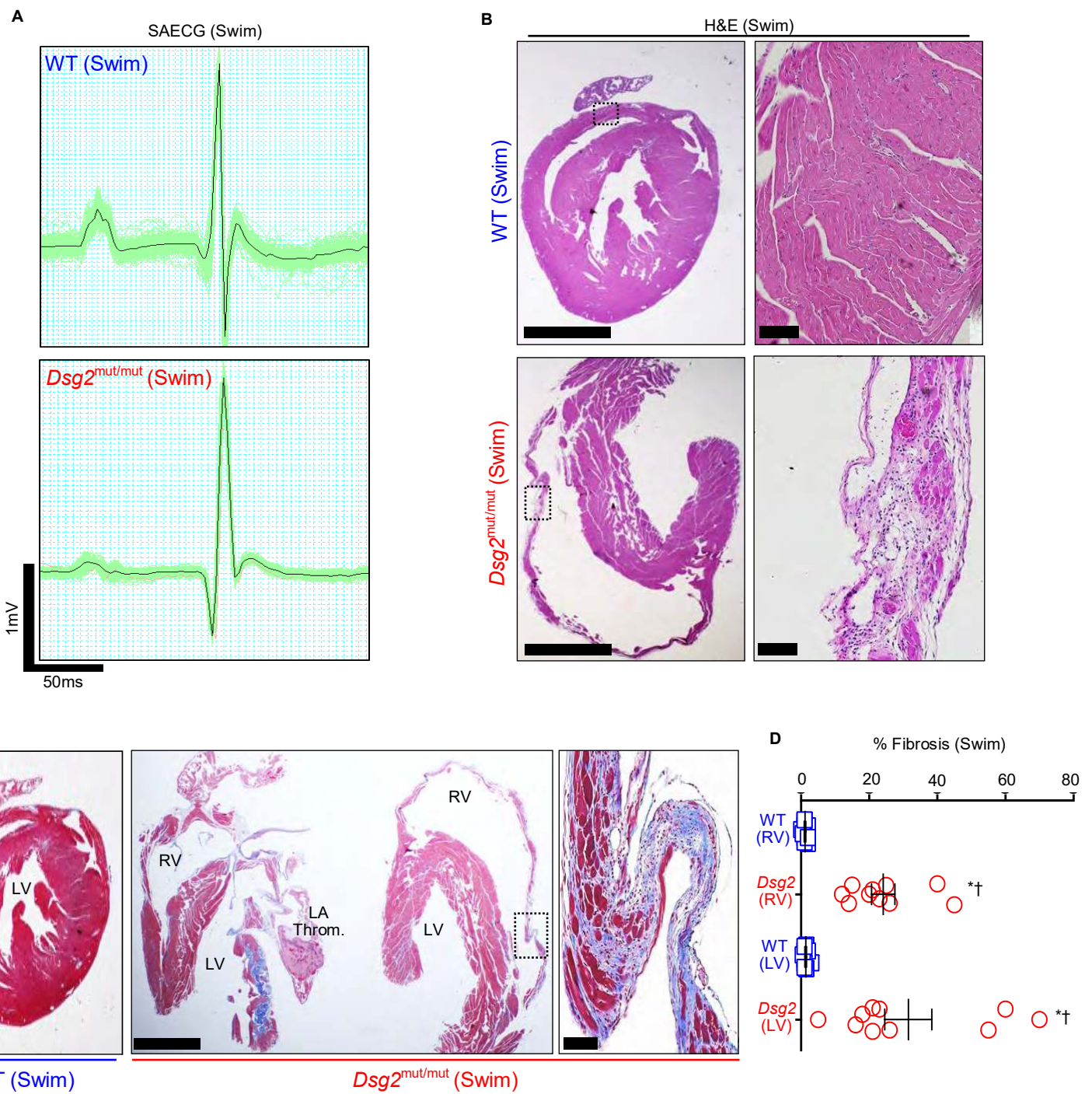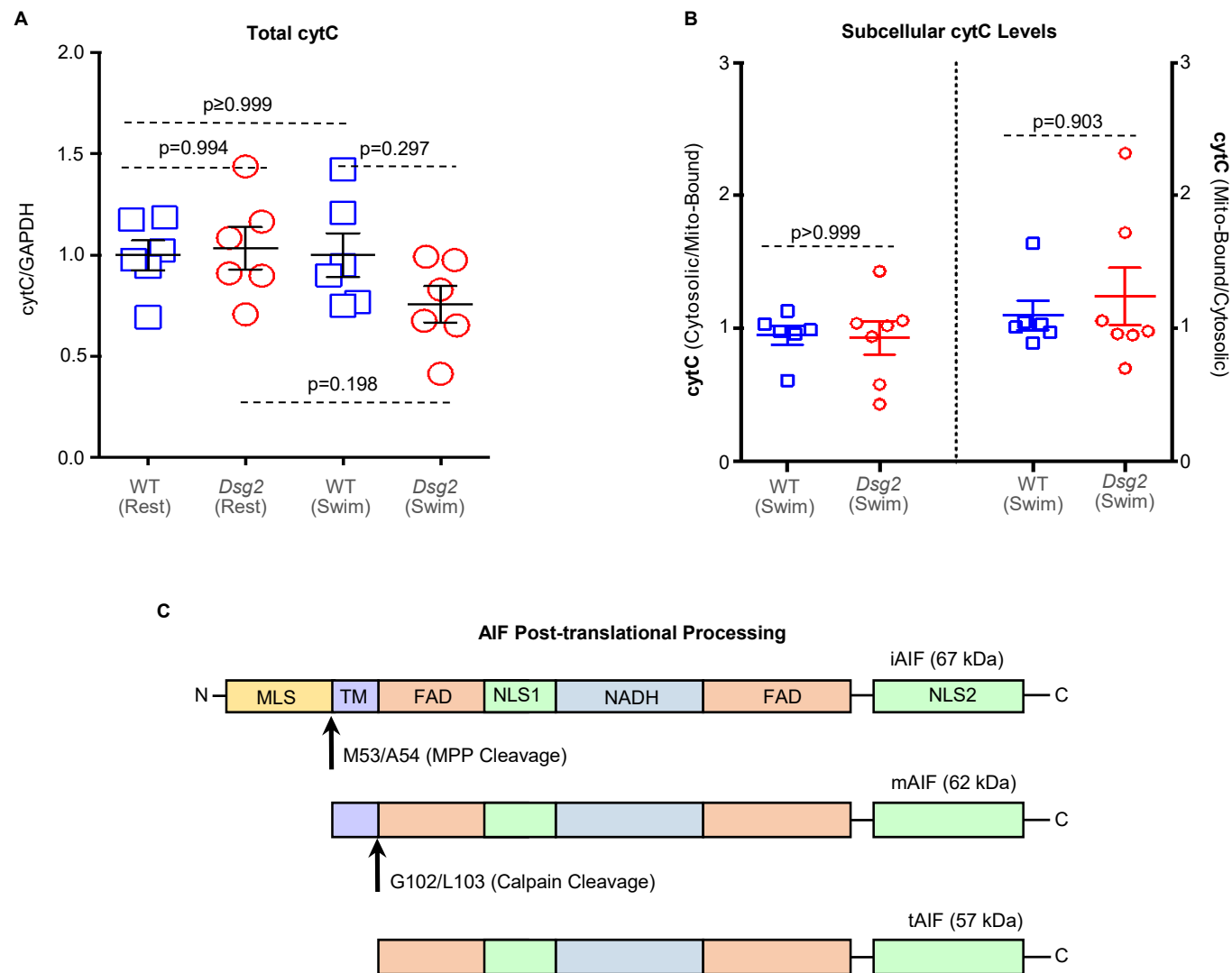
Supplementary Figure 1. *Dsg2*^mut/mut **mice display ECG abnormalities and myocardial injury in response to endurance exercise.** (**A**) Representative 90min signal averaged ECGs (SAECGs) from exercised mice at swim endpoint. Note, reduced S-amplitude and increased Q-amplitude from exercised *Dsg2*^mut/mut mice compared to WT mice. Representative of n≥13 mice/genotype. Scale bars inset, bottom left. (**B**) Exercised *Dsg2*^mut/mut myocardium displayed focal areas of inflammation/inflammatory infiltration as assessed via Hematoxylin & Eosin (H&E). (**C**) Masson's Trichrome stained myocardium from exercised mice. Note, diffuse epicardial-to-endocardial fibrosis throughout the RV, with highly localized epicardial-to-endocardial fibrotic lesions within the LV free wall from exercised *Dsg2*^mut/mut mice. Large scale bar = 1mm; small scale bar = 100µm; representative of n≥14 mice/genotype. Enlarged images are from dotted black boxes. LA Throm., left atrial thrombus. (**D**) *Dsg2*^mut/mut mice displayed increased %RV and %LV fibrosis compared to WT mice. Data presented as mean±SEM, n≥10 mice/genotype/parameter. *P<0.05 vs WT %LV fibrosis; †P<0.05 vs WT %RV fibrosis using One-way ANOVA with Tukey post-hoc.
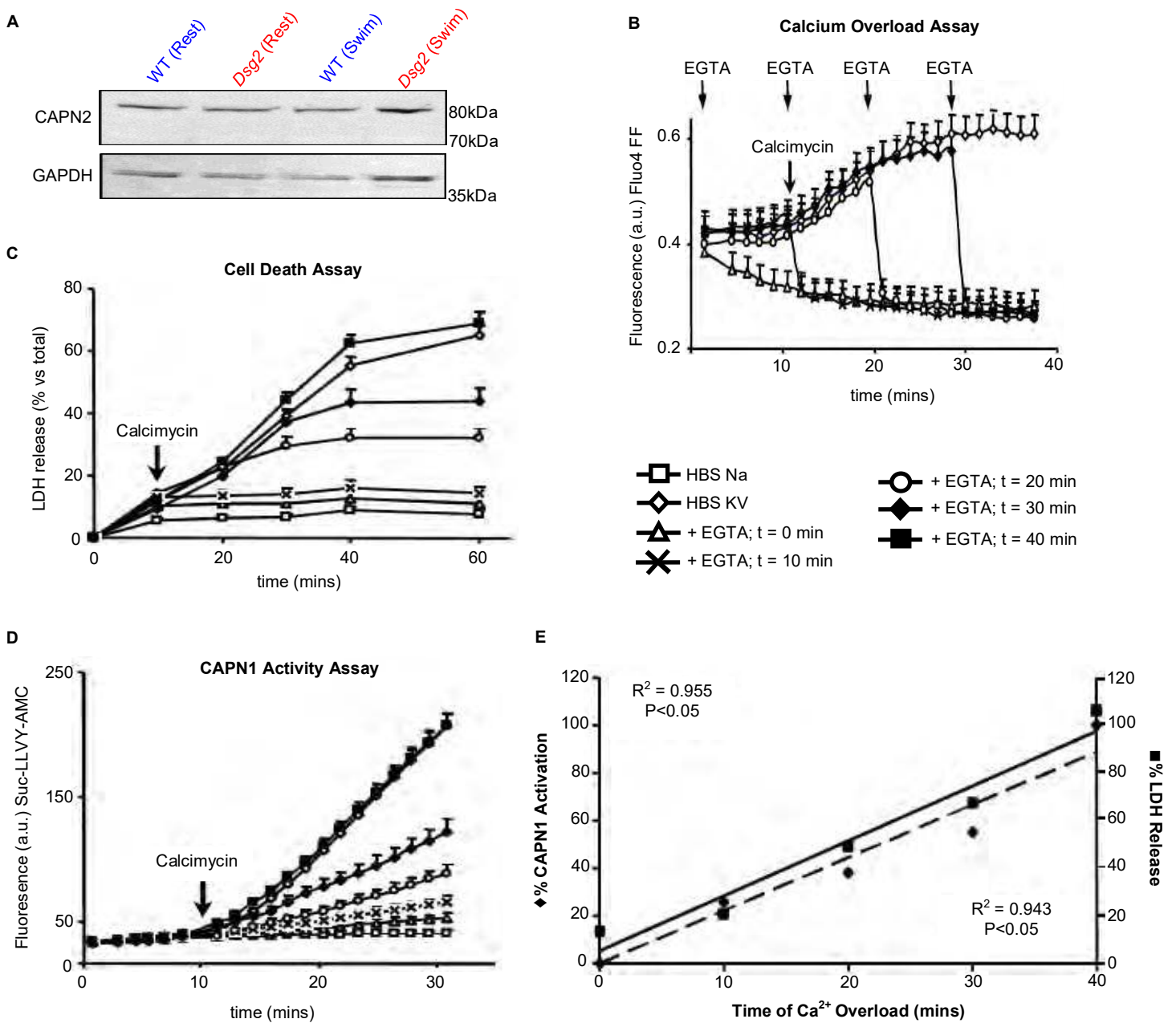
**Supplementary Figure 2. Calpain-1 activation and cell death in response to Ca^{2+} overload.** (**A**) Representative Calpain-2 (CAPN2) immunoblot showed no difference in myocardial CAPN2 expression from WT and *Dsg2$^{mut/mut}$*(*Dsg2*) mice, in sedentary and exercised cohorts. Representative of n=7/genotype/cohort. (**A-E**) HL-1 cells were exposed to Calcimycin (1µM, black arrows) to induce calcium (Ca^{2+}) overload, and the presence of the Ca^{2+} chelating agent, EGTA (5 mM) at different time points (indicated by the arrows). (**B**) Cytosolic Ca^{2+} overload was detected by loading HL-1 cells with 5 µM Fluo4 FF. EGTA addition induces a rapid decrease of Fluo4 FF fluorescence to baseline level. (**C**) Cell death was detected as LDH release. (**D**) CAPN1 activity was monitored via proteolytic fluorescent-cleavage of a synthetic CAPN1 peptide (Suc-LLVY-AMC). (**E**) Relationship between duration of Ca^{2+} overload (x-axis) with CAPN1 activation (%, solid diamonds; left y-axis) and with LDH release (%, solid squares; right y-axis). Data presented as mean±St.Dev., n=6 independent experiments/cohort, with n=3 cell culture replicates/condition. LDH release (right y-axis) and Suc-LLVY-AMC (%CAPN1 Activation, left y-axis) hydrolysis are expressed as percentage of the maximal value obtained after 40 min of intracellular Ca^{2+} overload. Pearson's r (R^2) correlation analyses and P-values inset.
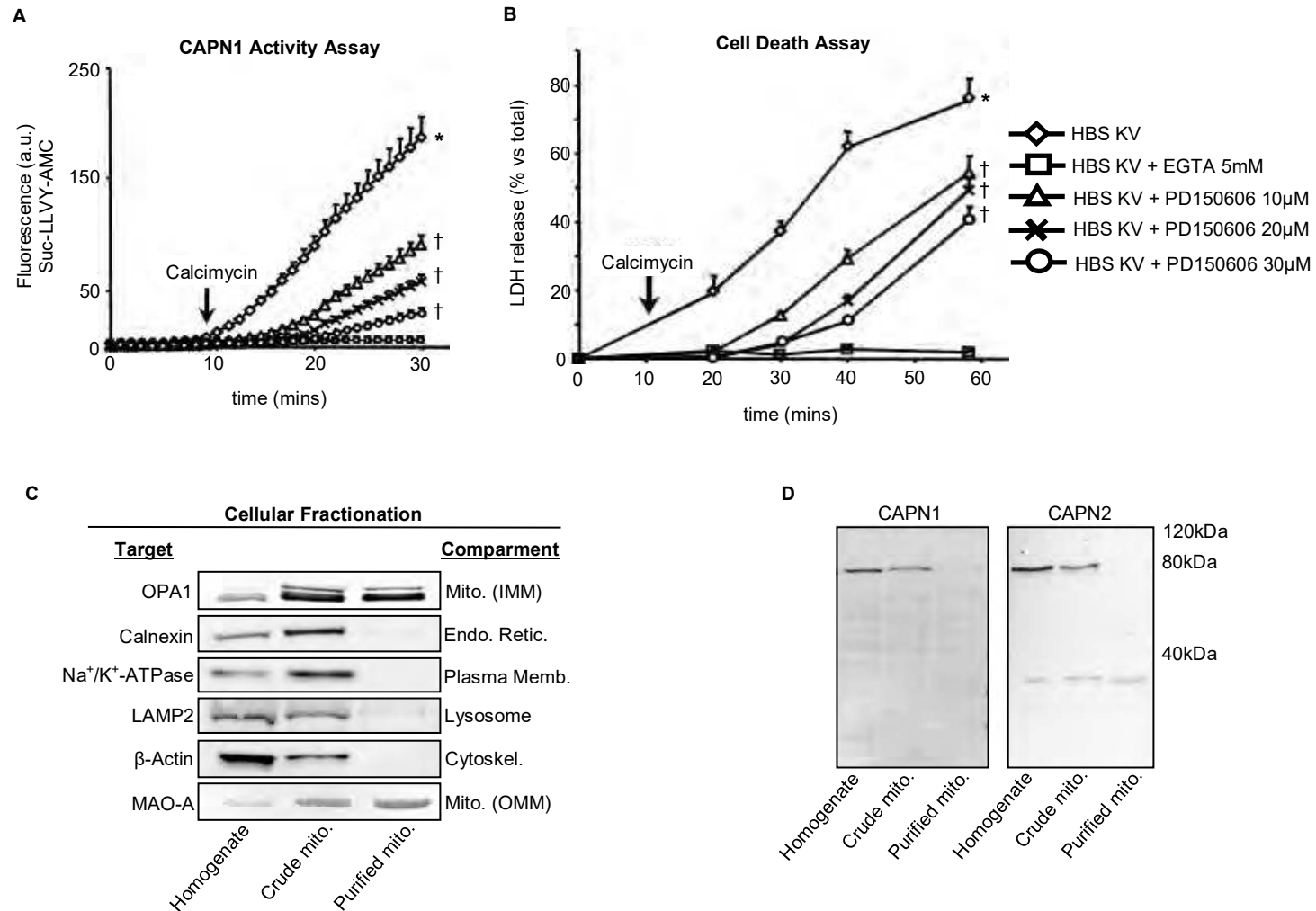
Supplementary Figure 3. Calpain-1 inhibition in HL-1 cells by PD150606. HL-1 cells were subjected to Ca^{2+} overload (via Calcimycin, black arrows) in HBS KV medium in the absence or presence of a PD150606 dose-dependent response. (**A**) CAPN1 activity was monitored by proteolysis of the synthetic peptide Suc-LLVY-AMC (25 μM). (**B**) Cell death was detected as LDH release. Data presented as mean±St.Dev., n=6 independent experiments/condition, with n=3 cell culture replicates/condition. *P<0.05 for HBS KV media vs all conditions; †P<0.05 for HBS KV PD1050606 (10, 20, and/or 30μM) media vs HBS KV media, using One-way ANOVA. (**C**) Crude and purified fractions of mitochondria were obtained from HL-1. Representative western blots of OPA1, calnexin, Na$^+$/K$^+$-ATPase, LAMP2, β-actin and MAO-A in protein extracts from total cell homogenate (lane 1), crude mitochondria (lane 2) and purified mitochondria (lane 3). Mito., mitochondria; IMM, inner mitochondrial membrane; Endo. Retic., endoplasmic reticulum; Plasma Memb., plasma membrane; Cytoskel., cytoskeleton; and OMM, outer mitochondrial membrane. (**D**) Representative western blots of Calpain-1 (CAPN1, left panel) or Calpain -2 (CAPN2, right panel) in protein extracts from total cell homogenate (lane 1), crude mitochondria (lane 2) and purified mitochondria (lane 3). For C, D, immunoblots are representative of n=6 independent experiments/condition, with n=3 cell culture replicates/condition.

Supplementary Figure 4. Cytochrome-C in *Dsg2*^{mut/mut} mice and post-translational modifications of AIF. (**A**) No differences in cytochrome-c (cytC) levels were observed between cohorts, at rest and in response to exercise (swim). Data presented as mean±SEM, n=6/cohort/condition, no significance to note using One-way ANOVA. (**B**) No differences in the cytosolic-to-mitochondrial bound cytC levels (left panel) or mitochondrial bound-to-cytosolic cytC levels were observed in subcellular fractions from exercised cohorts. Data presented as mean±SEM, n≥6 mice/cohort/condition, no significance to note using One-way ANOVA with Tukey's post-hoc. (**C**) Schematic showing immature AIF (iAIF) protein, post-translational processing by MPP (mitochondrial processing peptidase) which promotes binding of mature AIF (mAIF) to the mitochondria inner membrane space. Calpain-cleavage generates truncated AIF (tAIF). MLS, mitochondrial localization signal; TM, transmembrane sequence that binds to mitochondrial intermembrane space; FAD/NADH domains; NLS, nuclear localization signal; M, A, G, and L are amino acids methionine, alanine, glycine, and leucine, respectively.
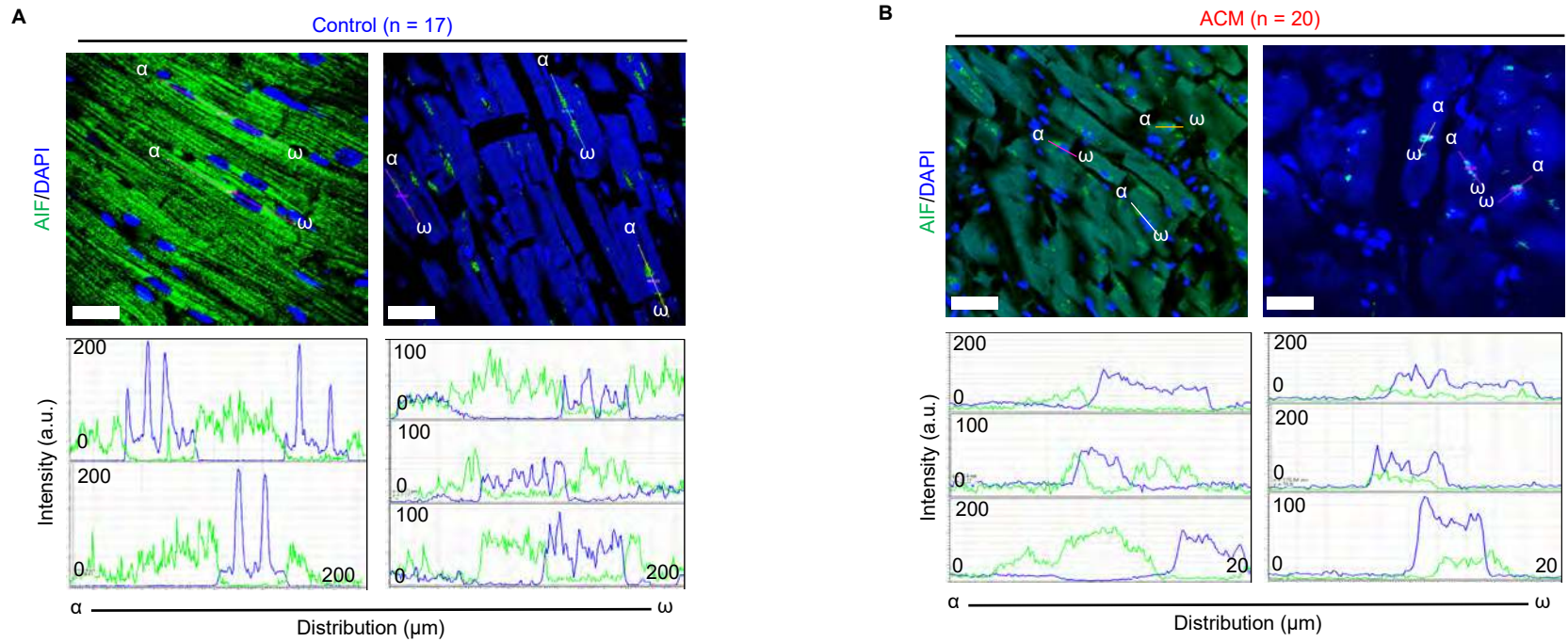
Supplementary Figure 5. AIF localization in ACM patient myocardium. Mitochondrial to nuclear AIF localization was assessed via confocal immunofluorescence microscopy analysis in myocardia obtained from individuals with (**A**) no history of heart disease at autopsy (i.e. controls, n=17) and compared against (**B**) myocardium from ACM patients (n=20). AIF-nuclear localization was confirmed via *fluorophore distribution vs fluorophore intensity* at 3-10 regions of interest (α-ω). Scale bars = 20 μm.
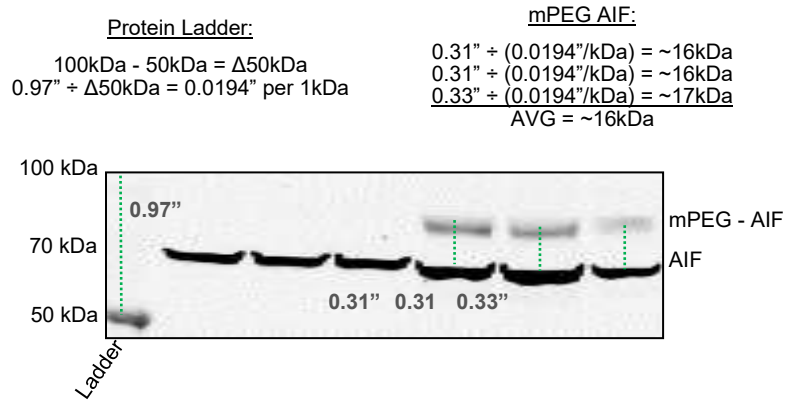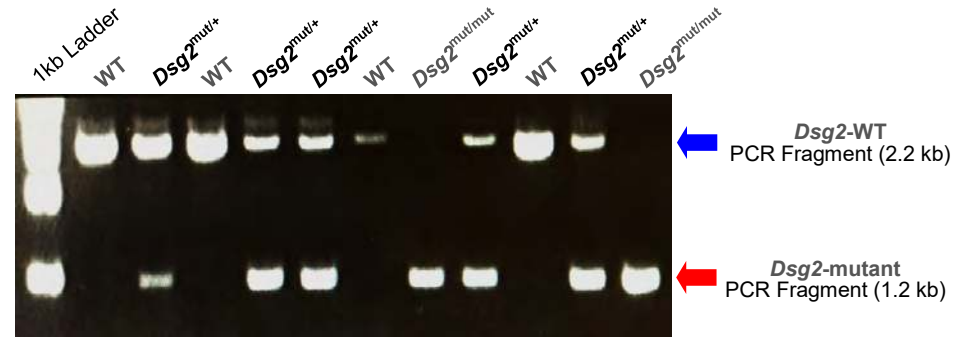
Supplementary Figure 6. Labeled cysteines and DNA gel electrophoresis. (**A**) Representative immunoblot with or without mPEG-treatment. The difference in 100-50kDa protein ladder (Δ50kDa) divided by the length (in inches) between 100-to-50kDa bands (0.97") was used to formulate the weight of mPEGged AIF. AIF contains 3 cysteines (regardless of its mature or truncated form). Representative immunoblot from WT mice (rest) showed that mPEG bound to each free cysteine of AIF, thus generated a ~15kDa shift in protein weight. More specifically, all three cysteines were not oxidized. (**B**) Representative gel electrophoresis following polymerase chain reaction (PCR) from age-matched littermate DNA samples. The control *Dsg2*-WT DNA fragment runs at 2.2kb and the *Dsg2*-mutant fragment runs at 1.2kb on a 1.5% agarose gel. Mice homozygous for mutant *Dsg2* (*Dsg2*$^{mut/mut}$) are labeled in red, mice heterozygous for mutant *Dsg2* (*Dsg2*$^{mut/+}$) are labeled in black, and WT mice are labeled in blue. PCR reaction primers, reagents and protocol for genotyping can be found in Chelko et al, *JCI Insight* 2016.

Parameter	WT	Dsg2[mut/mut]
Echocardiography		
n	20	15
IVSd (mm)	0.97 ± 0.02	0.78 ± 0.04*
IVSs (mm)	1.49 ± 0.04	1.08 ± 0.06*
LVIDd (mm)	2.80 ± 0.05	3.31 ± 0.19*
LVIDs (mm)	1.19 ± 0.06	2.24 ± 0.24*
RVIDd (mm)	1.16 ± 0.22	1.52 ± 0.52
RVIDs (mm)	0.42 ± 0.09	0.72 ± 0.28
LV-PWTd (mm)	0.94 ± 0.02	0.87 ± 0.03*
RV-PWTd (mm)	0.31 ± 0.03	0.32 ± 0.03
RV-EF (%)	65.5 ± 1.32	54.9 ± 4.25*
LV-EF (%)	81.6 ± 1.65	56.4 ± 4.79*
Electrocardiography		
n	13	13
PR-I (ms)	43.2 ± 2.1	45.7 ± 3.7
Pd (ms)	11.6 ± 0.7	10.8 ± 1.3
QRSd (ms)	16.7 ± 0.7	19.7 ± 1.1
P-Amp (mV)	0.10 ± 0.01	0.036 ± 0.01*
R-Amp (mV)	1.77 ± 0.13	1.49 ± 0.14
Q-Amp (mV)	-0.0003 ± 0.002	-0.12 ± 0.02*
S-Amp (mV)	-0.59 ± 0.07	-0.20 ± 0.03*
NSVT (Count)	4.85 ± 1.3	21.1 ± 6.3*

Supplementary Table 1. Echocardiographic and electrocardiographic indices from exercised WT and Dsg2[mut/mut] mice. IVS, interventricular septal end diastole (d) and end systole (s); LVID, left ventricular internal diameter; RVID, right ventricular internal diameter; LV-PWTd, LV posterior wall thickness; RV-PWTd, RV posterior wall thickness; PR-I, PR-Interval; Pd, P duration; QRSd, QRS duration; P-Amp, P-Amplitude; R-Amp, R-Amplitude; Q-Amp, Q-Amplitude; S-Amp, S-Amplitude. NSVT, non-sustained ventricular tachycardia. Data presented as mean±SEM, *n-values* inset, with a *$P<0.05$ vs. WT using 1-way ANOVA.

Supplementary Table 2. Desmosomal gene variants in ACM patients.

Gene (n)	Nucleotide Change	Amino Acid Change	No. of Patients (n = 14)
PKP2 (12)	c.2509delA	p.Ser837Valfs*94	2
	c.148_151delACAG	p.Thr50Serfs*61	3
	c.2146-1G>C	mutant splice product	1
	c.2013delC	p.Pro672fs*12	2
	c.2489+1G>A	mutant splice product	2
	c.2197_2202delCACACCinsG	p.His733Alafs*8	1
	c.235C>T	p.Arg79*	1
DSG2 (2)	c.523+2T>C	mutant splice product	1
	c.918G>A c.146G>A	p.Trp306* p.Arg49His	1[a]

PKP2, Plakophilin-2; *DSG2*, Desmoglein-2; [a]Indicates patient with a compound heterozygote mutation in *DSG2*.

Supplementary Table 3. Clinical characteristics and AIF-pathology scores in ACM patients.

ACM Cohort	Overall (n=20)	Desmosomal (14)	TFC (6)	P-value
AIF-immunostained score, mean ± SEM	2.85 ± 0.3	3.11 ± 0.3	2.25 ± 0.4	0.474
Clinical Phenotypes at Collection	**Overall (n=20)**	**Desmosomal (14)**	**TFC (6*)**	**P-value**
Proband, *n* (%)	13 (65)	9 (64)	4 (67)	>0.999
Structural alterations, *n* (%)	12 (60) major 5 (25) minor	10 (71) major 2 (14) minor	2 (33) major 3 (50) minor	>0.999
Repolarization abnormalities, *n* (%)	5 (25) major 9 (45) minor	4 (29) major 6 (43) minor	1 (17) major 3 (50) minor	>0.999
Depolarization abnormalities, *n* (%)	17 (85) major 0 (0) minor	14 (100) major 0 (0) minor	3 (50) major 0 (0) minor	0.297
Arrhythmias, *n* (%)	7 (35) major 10 (50) minor	6 (43) major 7 (50) minor	1 (17) major 3 (50) minor	0.950

TFC, Task Force Criteria (G-/P+ patients); Desmosomal (G+/P+ patients). Data presented as mean±SEM, n-values inset, P<0.05 via 2-way ANOVA, no significance to note.